INTERNATIONAL JOURNAL FOR NUMERICAL METHODS IN FLUIDS, VOL. 18, 1–26 (1994)

CO-LOCATED EQUAL-ORDER CONTROL-VOLUME FINITE ELEMENT METHOD FOR TWO-DIMENSIONAL AXISYMMETRIC INCOMPRESSIBLE FLUID FLOW

C. MASSON, H. J. SAABAS* AND B. R. BALIGA

Department of Mechanical Engineering, McGill University, Montréal, Québec, H3A 2K6, Canada

SUMMARY

The formulation of a control-volume-based finite element method (CVFEM) for axisymmetric, two-dimensional, incompressible fluid flow and heat transfer in irregular-shaped domains is presented. The calculation domain is discretized into torus-shaped elements and control volumes. In a longitudinal cross-sectional plane, these elements are three-node triangles, and the control volumes are polygons obtained by joining the centroids of the three-node triangles to the mid-points of the sides. Two different interpolation schemes are proposed for the scalar-dependent variables in the advection terms: a flow-oriented upwind function, and a mass-weighted upwind function that guarantees that the discretized advection terms contribute positively to the coefficients in the discretized equations. In the discretization of diffusion transport terms, the dependent variables are interpolated linearly. An iterative sequential variable adjustment algorithm is used to solve the discretized equations for the velocity components, pressure and other scalar-dependent variables of interest. The capabilities of the proposed CVFEM are demonstrated by its application to four different example problems. The numerical solutions are compared with the results of independent numerical and experimental investigations. These comparisons are quite encouraging.

KEY WORDS Axisymmetric flow Laminar flow Control-volume finite element method Mass-weighted skew upwind interpolation Flow-oriented upwind interpolation

1. INTRODUCTION

The main contribution of this paper is the formulation of a control-volume-based finite element method for two-dimensional *axisymmetric*, incompressible, viscous fluid flows. The proposed method is based on a primitive-variables, co-located, equal-order formulation: it works directly with the velocity components and pressure, these dependent variables are stored at the same nodes in the finite element mesh, and they are interpolated over the same elements.

The formulation of Control-Volume-based Finite Element Methods (CVFEMs) for fluid flow typically involves five basic steps: (i) discretization of the calculation domain into elements; (ii) further discretization of the calculation domain into control volumes that surround the nodes in the finite element mesh; (iii) prescription of element-based interpolation functions for the dependent variables and the thermophysical properties of the fluid; (iv) use of the subdomain, or control-volume-based, method of weighted residuals[1] and an element-by-element procedure to derive and assemble algebraic approximations to the governing equations; (v) prescription of

* Present Address: Project Engineer, Pratt and Whitney Canada Inc., Longueuil, Quebec J4X 4X9, Canada.

0271–2091/94/010001–26$18.00

Received 18 November 1992
Revised 20 May 1993

a procedure to solve these algebraic equations. Thus, CVFEMs combine concepts native to Finite Volume Methods (FVMs) and Finite Element Methods (FEMs). Indeed, following the views of Finlayson and Scriven[1] and Zienkiewicz,[2] FVMs, FEMs and CVFEMs can all be regarded as particular cases of the Method of Weighted Residuals (MWR).

In the mid-1970s, the desire and the need to extend the capabilities of the successful Marker And Cell (MAC) method of Harlow and Welch,[3] and the FVMs of Patankar and Spalding,[4] and Raithby[5] to irregular geometries provided the motivation for the CVFEMs of Baliga,[6] Ramadhyani[7] and Prakash.[8] These early CVFEMs were formulated by combining and extending concepts borrowed from the aforementioned FVMs, the work of Winslow,[9] and the FEMs of Zienkiewicz,[2] Oden,[10] and Taylor and Hood.[11] Today, many papers dealing with the formulation and application of CVFEMs for conduction, convection–diffusion and fluid flow problems are available in published literature. Examples include the works of Baliga and Patankar,[12-14] Prakash and Patankar,[15] LeDain-Muir and Baliga,[16] Prakash,[17] Hookey and Baliga,[18] Schneider and Raw,[19,20] Costa and Oliviera[21] and Elkaim *et al.*[22] The combination of finite element and finite volume approaches can also be found in the works of Choudhury and Nicolaides,[23] van Leer,[24] Jameson and Mavriplis,[25] Lahrmann[26] and Swaminathan and Voller.[27]

Recent reviews of CVFEMs for two- and three-dimensional viscous fluid flows are available in the works of Hookey,[28] Saabas[29] and Baliga and Saabas.[30] Most of the CVFEMs proposed in the 1970s and 1980s have intrinsic difficulties that restrict the scope of their applicability to practical problems. CVFEMs based on flow-oriented upwind schemes[12,16,17] are successful in reducing the false diffusion that afflicts locally one-dimensional upwind schemes used in FVMs,[31] but they can encounter difficulties caused by negative coefficients in the discretization equations. These difficulties can become quite serious when obtuse-angled triangular elements, or tetrahedral elements with a solid angle exceeding $\pi/2$ steradians, are used in problems that involve *high Peclet numbers*:[29,30] furthermore, for these conditions, additional difficulties related to indeterminate coefficients in the interpolation functions may be encountered.[29] Some of the two-dimensional CVFEMs based on unequal-order and equal-order co-located formulations are successful in avoiding checkerboard-type pressure distributions in incompressible flow problems, but they suffer from other difficulties: the unequal-order formulation of Baliga and Patankar[13] can suffer a loss of accuracy in problems with high Reynolds numbers, and its extension to three dimensions would be quite cumbersome; the co-located equal-order formulations of Prakash[17] and Hookey and Baliga[18] require overspecification of boundary conditions and encounter convergence difficulties in problems with inflow and outflow boundaries.[29] Schneider and Raw[19,20] have proposed a co-located equal-order CVFEM based on a mass-weighted upwind scheme. This method ensures that the discretized convective transport terms contribute positively to the coefficients in the discretization equations, and it avoids spurious oscillations in the computed pressure field. However, this CVFEM[19,20] is based on planar quadrilateral elements, and its behaviour in problems with inflow and outflow boundaries has not been discussed in detail in the published literature.

The recently completed work of Saabas[29] was aimed at overcoming some of the difficulties mentioned earlier. It has resulted in an equal-order co-located CVFEM that deals directly with primitive variables and is capable of solving steady, multidimensional, laminar and turbulent, incompressible, viscous fluid flow problems in irregular-shaped geometries, with or without inflow and outflow boundaries.[29,30] During the work of Saabas,[29] it appeared as if there was no published description of a primitive-variables-based CVFEM for the solution of *two-dimensional axisymmetric* fluid flow problems. The work described in this paper was undertaken to develop such a CVFEM, by adapting and extending ideas contained in earlier methods.[12,15,19,29] In this

context, it should be noted that a recently published paper by Elkaim *et al.*[22] does discuss a CVFEM for two-dimensional axisymmetric flows, but it is based on a stream function–vorticity formulation. Furthermore, Elkaim *et al.*[22] present a mathematical model and results for two-dimensional axisymmetric flow problems, but their numerical solution procedure is described in the context of a two-dimensional planar (Cartesian) formulation akin to the CVFEM of Baliga and Patankar.[12]

The formulation of the proposed two-dimensional axisymmetric CVFEM is presented in Section 3. Following that, the capabilities of this CVFEM are demonstrated by its application to four different example problems.

2. GOVERNING EQUATIONS

With respect to the cylindrical co-ordinate system (r, θ, z), steady, axisymmetric, elliptic flows of Newtonian fluids are governed by the following differential equations:

z-momentum equation

$$\frac{\partial}{\partial z}(\rho uu)+\frac{1}{r}\frac{\partial}{\partial r}(r\rho vu)=-\frac{\partial p}{\partial z}+\frac{\partial}{\partial z}\left(\mu\frac{\partial u}{\partial z}\right)+\frac{1}{r}\frac{\partial}{\partial r}\left(r\mu\frac{\partial u}{\partial r}\right)+S_z, \tag{1}$$

r-momentum equation

$$\frac{\partial}{\partial z}(\rho uv)+\frac{1}{r}\frac{\partial}{\partial r}(r\rho vv)=-\frac{\partial p}{\partial r}+\frac{\partial}{\partial z}\left(\mu\frac{\partial v}{\partial z}\right)+\frac{1}{r}\frac{\partial}{\partial r}\left(r\mu\frac{\partial v}{\partial r}\right)-\mu\frac{v}{r^2}+S_r, \tag{2}$$

continuity equation

$$\frac{\partial}{\partial z}(\rho u)+\frac{1}{r}\frac{\partial}{\partial r}(r\rho v)=0, \tag{3}$$

other conservation equations (general form)

$$\frac{\partial}{\partial z}(\rho u\phi)+\frac{1}{r}\frac{\partial}{\partial r}(r\rho v\phi)=\frac{\partial}{\partial z}\left(\Gamma_\phi\frac{\partial \phi}{\partial z}\right)+\frac{1}{r}\frac{\partial}{\partial r}\left(r\Gamma_\phi\frac{\partial \phi}{\partial r}\right)+S_\phi. \tag{4}$$

In these equations, ρ is the mass density of the fluid, p is the pressure, μ is the dynamic viscosity of the fluid, u and v are the velocity components in the z- and r-directions, respectively, and S_z and S_r are the corresponding volumetric source terms. In equation (4), ϕ can be used to represent any scalar-dependent variable, such as temperature, mass concentration, kinetic energy of turbulence and its dissipation rate; Γ_ϕ is the corresponding diffusion coefficient; and S_ϕ is the appropriate volumetric source term.

The momentum and the continuity equations, equations (1)–(3), can be obtained from equation (4) by defining the dependent variable, ϕ, the diffusion coefficient, Γ_ϕ, and source term, S_ϕ, according to Table I.

3. PROPOSED METHOD

This method was constructed by adapting and extending ideas from CVFEMs proposed by Baliga and Patankar,[12–14] Prakash and Patankar,[15] Schneider and Raw[19,20] and Saabas.[29] Concise descriptions of the various steps involved in the formulation of the proposed CVFEM are presented in this section.

Table I. Specific forms of the general equation

	Γ_ϕ	ϕ	S_ϕ
z-momentum	μ	u	$S_z-(\partial p/\partial z)$
r-momentum	μ	v	$S_r-(\partial p/\partial r)-\mu v/r^2$
Continuity	0	1	0

3.1. Domain discretization

It is convenient to present the domain discretization procedure with respect to a longitudinal cross-section of the axisymmetric domain of interest. This cross-section is first divided into three-node triangular elements. Then the centroids of the elements are joined to the midpoints of the corresponding sides. This creates polygonal control volumes around each node in the finite element mesh. The longitudinal cross-section of a sample domain discretization is shown in Figure 1; the solid lines denote the domain and element boundaries, the dashed lines represent the control-volume faces and the shaded areas show the control volumes associated with one internal node and one boundary node.

The discretization of the longitudinal cross-section is rotated through 2π radians about the axis of symmetry. The result is a discretization of the axisymmetric calculation domain into torus elements of triangular cross-section, and torus control volumes of polygonal cross-section. In the rest of the paper, for conciseness in the presentation, the torus elements and torus control volumes will be referred to as triangular (three-node) elements and polygonal control volumes, respectively.

3.2. Integral conservation equation

Consider a typical node i in the calculation domain: it could be an internal node, such as the one shown in Figure 2(a), or a boundary node, similar to the one shown in Figure 2(b). An integral formulation corresponding to equation (4) can be obtained by applying the appropriate conservation principle for the dependent variable, ϕ, to a suitably chosen control volume. The resulting integral conservation equation, when applied to the control volume surrounding node i in Figure 2, can be written as follows:

$$\left[\int_a^o \mathbf{J}\cdot\mathbf{n}2\pi r\,\mathrm{d}s+\int_o^c \mathbf{J}\cdot\mathbf{n}2\pi r\,\mathrm{d}s-\int_{iaoc} S_\phi\,\mathrm{d}\mathscr{V}\right]$$
$$+[\text{similar contributions from other elements associated with node } i]$$
$$+[\text{boundary contributions, if applicable}]=0, \tag{5}$$

where $\mathbf{n}$ is a unit outward vector normal to the differential length element, ds, and $\mathbf{J}$ is the combined convection–diffusion flux of ϕ:

$$\mathbf{J}=\mathbf{J}_\mathrm{D}+\mathbf{J}_\mathrm{C}, \tag{6}$$

$$\mathbf{J}_\mathrm{D}=-\Gamma_\phi\nabla\phi, \tag{7}$$

$$\mathbf{J}_\mathrm{C}=\rho\mathbf{V}\phi. \tag{8}$$

The form of equation (5) emphasizes that it can be assembled by using an element-by-element procedure.

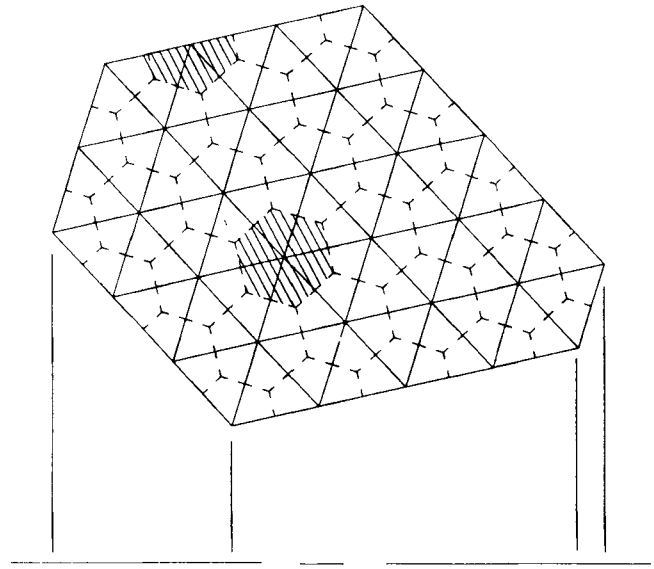

Figure 1. Discretization of the longitudinal cross-section of a calculation domain

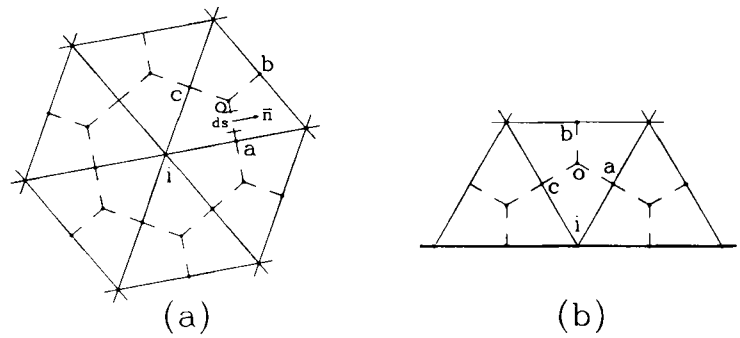

Figure 2. Cross-sections of typical control volumes associated with (a) an internal node (b) a boundary node

3.3. Interpolation functions

The derivation of algebraic approximations to the integral conservation equations requires the specification of element-based interpolation functions for the dependent variable, ϕ, diffusion coefficient, Γ_ϕ, source terms, S_ϕ, and mass density, ρ.

The interpolation functions are specific to each element. For convenience, in the formulation of these functions, in each element, a local (x, y) co-ordinate system is defined such that the origin is at the centroid of the triangular element, the x-axis is in the direction of z, and the y-axis is in the direction of r. The interpolation functions will be expressed with respect to this local co-ordinate system.

Diffusion coefficient, density and sources. In each triangular element, the centroidal value of Γ_ϕ and ρ are assumed to prevail over the corresponding element.

The source term, S_ϕ, is linearized, if required, and expressed in the following general form:[31]

$$S_\phi = S_C + S_P \phi. \tag{9}$$

In each element, the values of S_C and S_P are computed at the nodes and assumed to prevail over the portions of the corresponding control volumes that lie within the element.

Mass flow rates. In the calculation of mass flow rates across the control volume faces, the velocity is interpolated in a special way in each element, and this mass-flow related velocity is denoted by

$$\mathbf{V}^m = u^m \mathbf{i} + v^m \mathbf{j}. \tag{10}$$

This special treatment, borrowed from the work of Prakash and Patankar,[15] prevents the occurrence of spurious pressure oscillations in the proposed co-located equal-order CVFEM. The development of this interpolation is based on the discretized momentum conservation equations. Therefore, it will be presented later in this paper.

ϕ in diffusion terms. In the derivation of algebraic approximations to surface integrals of diffusion fluxes, equations (5) and (7), the dependent variable ϕ is interpolated linearly in each element:

$$\phi = Ax + By + C. \tag{11}$$

Referring to Figure 3(a), the constants A, B and C can be uniquely determined in terms of the x, y co-ordinates of the three nodes, and the corresponding values of ϕ. Thus, with reference to the element 123 and the local x, y co-ordinate system shown in Figure 3(a),

$$A = [(y_2 - y_3)\phi_1 + (y_3 - y_1)\phi_2 + (y_1 - y_2)\phi_3]/\mathrm{DET}, \tag{12}$$

$$B = [(x_3 - x_2)\phi_1 + (x_1 - x_3)\phi_2 + (x_2 - x_1)\phi_3]/\mathrm{DET}, \tag{13}$$

$$C = [(x_2 y_3 - x_3 y_2)\phi_1 + (x_3 y_1 - x_1 y_3)\phi_2 + (x_1 y_2 - x_2 y_1)\phi_3]/\mathrm{DET}, \tag{14}$$

where

$$\mathrm{DET} = (x_1 y_2 + x_2 y_3 + x_3 y_1 - y_1 x_2 - y_2 x_3 - y_3 x_1). \tag{15}$$

An equivalent, and perhaps more elegant, development of this linear interpolation on triangular elements could be done using barycentric or area co-ordinates, traditionally employed in FEMs.[2] It should also be noted that with such linear interpolation functions, Delauney triangulation is

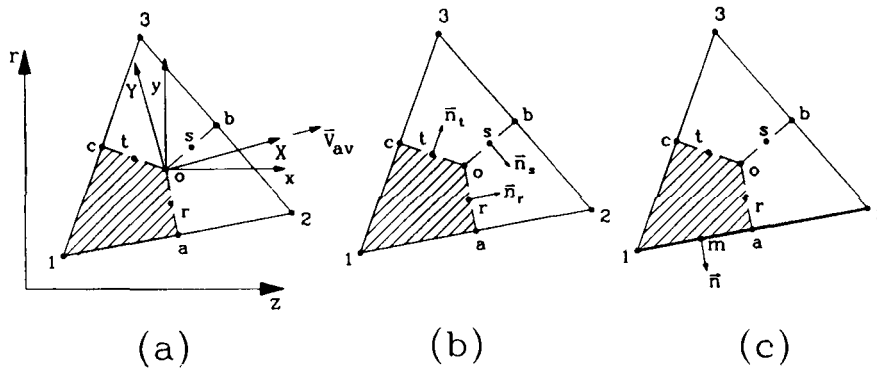

Figure 3. Cross-section of a typical triangular element, and notation used in the formulation

required to ensure that algebraic approximations of the diffusion transport terms contribute positively to the coefficients in the discretized equations. Barth[32] has presented a formal proof of this statement for two-dimensional planar problems.

ϕ in convection terms. In the derivation of algebraic approximations to surface integrals of the convective fluxes, equations (5) and (8), two different interpolation schemes for ϕ were investigated: a Flow-Oriented upwind scheme (FLO) and a Mass-Weighted upwind scheme (MAW).

The FLO scheme is based on the earlier work of Baliga and Patankar.[12,14] The interpolation function used in this scheme responds appropriately to an element-based Peclet number and to the direction of the element-average velocity vector. This interpolation function for ϕ is defined using a local flow-oriented co-ordinate system (X, Y) as shown in Figure 3(a): the origin of this co-ordinate system is located at the centroid of the element, and the X-axis is oriented along the element-average velocity, $\mathbf{V}_{\mathrm{av}}^m$:

$$\phi = A\xi + BY + C, \tag{16}$$

where

$$\xi = \frac{\Gamma_\phi}{\rho U_{\mathrm{av}}^m}\left\{\exp\left[\frac{Pe_\Delta(X - X_{\max})}{X_{\max} - X_{\min}}\right] - 1\right\}, \tag{17}$$

$$Pe_\Delta = \rho U_{\mathrm{av}}^m \frac{X_{\max} - X_{\min}}{\Gamma_\phi}, \tag{18}$$

$$X_{\max} = \max(X_1, X_2, X_3), \qquad X_{\min} = \min(X_1, X_2, X_3), \tag{19}$$

$$U_{\mathrm{av}}^m = |\mathbf{V}_{\mathrm{av}}^m|. \tag{20}$$

The constants A, B and C in equation (16) can be determined from equations (12)–(15) with the following modifications: replace x_1, x_2 and x_3 by ξ_1, ξ_2 and ξ_3, respectively, and replace y_1, y_2 and y_3 by Y_1, Y_2 and Y_3, respectively. It should be noted that with reference to the typical element shown in Figure 3(a), the element-average value of velocity in equation (20), $\mathbf{V}_{\mathrm{av}}^m$, is given by

$$\mathbf{V}_{\mathrm{av}}^m = u_{\mathrm{av}}^m \mathbf{i} + v_{\mathrm{av}}^m \mathbf{j}, \tag{21}$$

where $\mathbf{i}$ and $\mathbf{j}$ are unit vectors in the z- and r-directions, respectively, and

$$u_{\mathrm{av}}^m = \frac{u_1^m + u_2^m + u_3^m}{3}, \qquad v_{\mathrm{av}}^m = \frac{v_1^m + v_2^m + v_3^m}{3}, \tag{22}$$

with u_i^m and v_i^m computed using equation (48). In planar two-dimensional problems that involve acute-angled triangular elements and relatively low element-based Peclet numbers, the FLO scheme has proved quite successful.[12,29] If high values of the element Peclet number are encountered, however, the FLO scheme can lead to negative coefficients in the algebraic discretized equations,[12,29] and this difficulty is compounded when obtuse-angled triangular elements are used. These negative coefficients imply that an increase in the value of the transported scalar at a node outside the corresponding control volume can lead to an increase in the net outflow of the scalar from that control volume. This is physically incorrect. In steady-state problems, in the absence of source terms, for a scalar to be transported out of a control volume, it first has to flow into the control volume.[33] The donor-cell scheme of Prakash[34] is one way of ensuring positive coefficients: in this approach, the value of a scalar convected out of a control volume, across its surface, is set equal to the value of the scalar at the node within the control volume. This approach guarantees positive coefficients, but takes little account of the influence of the direction of the flow. Thus, it is prone to considerable false diffusion.[34]

The proposed MAW scheme is an adaptation of the positive-coefficient schemes of Schneider and Raw[19] and Saabas.[29] It ensures, at the element level, that the extent to which the dependent variable at a node exterior to a control volume contributes to the convective outflow is less than or equal to its contribution to the inflow by convection. Thus, it is a sufficient condition to ensure that the algebraic approximations to the convective terms in equation (5) add positively to the discretized equation. Furthermore, the MAW scheme takes better account of the influence of the direction of the flow than the donor-cell scheme of Prakash.[34] Thus, the MAW scheme produces less false diffusion than the donor-cell scheme.

The MAW scheme defines a mass-weighted average of ϕ at each of the three control surfaces of a triangular element (Figure 3(b)), namely, ϕ_r, ϕ_s, ϕ_t, in the following manner.

Let

$$\dot{m}_r = \int_o^a \rho \mathbf{V}^m \cdot \mathbf{n}_r 2\pi r \, ds, \qquad \dot{m}_s = \int_o^b \rho \mathbf{V}^m \cdot \mathbf{n}_s 2\pi r \, ds, \qquad \dot{m}_t = \int_o^c \rho \mathbf{V}^m \cdot \mathbf{n}_t 2\pi r \, ds, \tag{23}$$

where $\mathbf{n}_r, \mathbf{n}_s$ and $\mathbf{n}_t$ are unit normals, defined in Figure 3(b):

$$\phi_r = \begin{cases} f_p\phi_t + (1-f_p)\phi_1, & \text{where } f_p = \min[\max(-\dot{m}_t/\dot{m}_r, 0), 1] \text{ if } \dot{m}_r > 0, \\ f_p\phi_s + (1-f_p)\phi_2, & \text{where } f_p = \min[\max(-\dot{m}_s/\dot{m}_r, 0), 1] \text{ if } \dot{m}_r < 0, \end{cases} \tag{24}$$

$$\phi_s = \begin{cases} f_p\phi_t + (1-f_p)\phi_3, & \text{where } f_p = \min[\max(\dot{m}_t/\dot{m}_s, 0), 1] \text{ if } \dot{m}_s > 0, \\ f_p\phi_r + (1-f_p)\phi_2, & \text{where } f_p = \min[\max(-\dot{m}_r/\dot{m}_s, 0), 1] \text{ if } \dot{m}_s < 0, \end{cases} \tag{25}$$

$$\phi_t = \begin{cases} f_p\phi_r + (1-f_p)\phi_1, & \text{where } f_p = \min[\max(-\dot{m}_r/\dot{m}_t, 0), 1] \text{ if } \dot{m}_t > 0, \\ f_p\phi_s + (1-f_p)\phi_3, & \text{where } f_p = \min[\max(\dot{m}_s/\dot{m}_t, 0), 1] \text{ if } \dot{m}_t < 0, \end{cases} \tag{26}$$

These mass-weighted averages of ϕ are assumed to prevail over each control surface when the surface integrals of the convection terms, equations (5) and (8), are evaluated. The algebraic approximations of the mass flow rates in equation (23) will be discussed later.

In problems with acute-angled triangular elements and relatively low-element Peclet numbers, the FLO scheme is more accurate than the MAW scheme. As was mentioned earlier, however, when high element-based Peclet numbers are involved, especially in conjuction with obtuse-angled elements, the FLO scheme produces negative coefficients in the discretized equations. Negative coefficients in the discretized equations can lead to the following difficulties: (i) the numerical solutions could exhibit spurious oscillations about the exact solution; (ii) iterative solution algorithms could diverge; (iii) in problems involving always-positive dependent variables, such as concentration of a chemical species or phase, or the kinetic energy of turbulence, physically meaningless solutions or divergence could result. When such difficulties are encountered, the MAW scheme is recommended. Indeed, a formulation that automatically switches from the FLO scheme to the MAW scheme, when necessary, could be conceived, but this is not within the scope of this paper.

The MAW scheme defined by equations (23)–(26) is highly implicit. This does not pose any special difficulties in the proposed derivation of the discretization equations, as presented in the next section, because it is based on successive substitution, or Picard, linearization of the convective transport terms in the momentum equations. However, the MAW scheme would make Newton-type linearizations very difficult. It should also be noted that in this scheme, to obtain expressions for ϕ_r, ϕ_s and ϕ_t in terms of ϕ_1, ϕ_2 and ϕ_3, a 3×3 matrix of element-interpolation coefficients must be inverted. Further details are available in the work of Saabas.[29]

Pressure p. Pressure is interpolated linearly in each element. With respect to the local x–y co-ordinate system shown in Figure 3(a),

$$p = dx + ey + f. \tag{27}$$

The constants d, e and f can be obtained using procedures similar to those used to determine the constants A, B and C in equations (12)–(14).

3.4. *Discretization equations*

The discretization equations are obtained by first deriving algebraic approximations to the element contributions and the boundary contributions, if applicable, and then assembling these contributions appropriately.

Discretization equation for ϕ.

The following discussion pertains to node 1 of the element shown in Figure 3. The element contribution consists of the diffusion, convection and source contributions. The derivation of algebraic approximations to each of these contributions is presented separately.

Diffusion contribution. In each element, the diffusion flux $\mathbf{J}_D$ can be expressed in terms of its components in the z- and r-directions:

$$\mathbf{J}_D = J_{Dz}\mathbf{i} + J_{Dr}\mathbf{j} = \left(-\Gamma_\phi \frac{\partial \phi}{\partial x}\right)\mathbf{i} + \left(-\Gamma_\phi \frac{\partial \phi}{\partial y}\right)\mathbf{j}, \tag{28}$$

where $\mathbf{i}$ and $\mathbf{j}$ are unit vectors in the z- and r-directions, respectively. The interpolation function given in equation (11) is used to approximate J_{Dz} and J_{Dr}. Thus, with reference to element 123 and the local co-ordinate system in Figure 3(a), the diffusion contribution is approximated as follows:

$$\int_a^o \mathbf{J}_D \cdot \mathbf{n} 2\pi r \, ds = 2\pi \frac{r_o + r_a}{2} [\Gamma_\phi A y_a - \Gamma_\phi B x_a], \tag{29}$$

$$\int_o^c \mathbf{J}_D \cdot \mathbf{n} 2\pi r \, ds = 2\pi \frac{r_o + r_c}{2} [-\Gamma_\phi A y_c + \Gamma_\phi B x_c], \tag{30}$$

where A and B are given by equations (12) and (13), respectively.

Convection contribution. In each element, the convection flux $\mathbf{J}_C$ can be expressed in terms of its components in the z- and r-directions:

$$\mathbf{J}_C = J_{Cz}\mathbf{i} + J_{Cr}\mathbf{j} = \rho u^m \phi \mathbf{i} + \rho v^m \phi \mathbf{j}, \tag{31}$$

where ϕ is given by equation (16) when the FLO scheme is used, or equations (24)–(26) when using the MAW scheme. It should be noted here again that u^m and v^m denote components of the velocity vector, $\mathbf{V}^m$, in the mass-flux terms.

In the case of the FLO scheme, the interpolation function given in equation (16) is used to approximate ϕ, equation (48) is used to obtain u^m and v^m, and the convection contribution is evaluated using Simpson's rule as follows:

$$\int_a^o \mathbf{J}_C \cdot \mathbf{n} 2\pi r \, ds = 2\pi \left\{ -\frac{y_a}{6} [r_o (J_{Cz})_o + 4 r_r (J_{Cz})_r + r_a (J_{Cz})_a] + \frac{x_a}{6} [r_o (J_{Cr})_o + 4 r_r (J_{Cr})_r + r_a (J_{Cr})_a] \right\}, \tag{32}$$

$$\int_o^c \mathbf{J}_C \cdot \mathbf{n} 2\pi r \, ds = 2\pi \left\{ +\frac{y_c}{6} [r_o (J_{Cz})_o + 4 r_t (J_{Cz})_t + r_c (J_{Cz})_c] - \frac{x_c}{6} [r_o (J_{Cr})_o + 4 r_t (J_{Cr})_t + r_c (J_{Cr})_c] \right\}. \tag{33}$$

When the MAW scheme is used, the convection contribution is simply expressed as

$$\int_a^o \mathbf{J}_C \cdot \mathbf{n} 2\pi r \, ds = \dot{m}_r \phi_r \qquad \int_o^c \mathbf{J}_C \cdot \mathbf{n} 2\pi r \, ds = \dot{m}_l \phi_l. \tag{34}$$

It should be noted that $\dot{m}_r$ and $\dot{m}_l$ are mass flow rates across the corresponding control surfaces, in the directions of the normals $\mathbf{n}_r$ and $\mathbf{n}_l$, respectively (see Figure 3(b)), as expressed in equation (23).

Source term. The volume integral involving the source term S_ϕ is approximated as follows:

$$\int_{1aoc} S_\phi \, d\mathscr{V} = S_{C1} \mathscr{V}_{1aoc} + S_{P1} \phi_1 \mathscr{V}_{1aoc}, \tag{35}$$

where S_{C1}, S_{P1} are the values of S_C and S_P associated with node 1 in the element of interest, and

$$\mathscr{V}_{1aoc} = 2\pi \frac{|\mathrm{DET}|}{36}(2r_1 + 2r_o + r_a + r_c), \tag{36}$$

where DET is given by equation (15).

Adding up the diffusion, convection and source contributions, the total contribution of element 123 to the conservation equation for node 1 is obtained. The algebraic approximation to this total element contribution can be compactly expressed as follows:

$$\int_a^o \mathbf{J} \cdot \mathbf{n} 2\pi r \, ds + \int_o^c \mathbf{J} \cdot \mathbf{n} 2\pi r \, ds - \int_{1aoc} S_\phi \, d\mathscr{V} = C_1^\phi \phi_1 + C_2^\phi \phi_2 + C_3^\phi \phi_3 + D^\phi. \tag{37}$$

Expressions similar to equation (37) can be derived for the contributions of all elements associated with the internal node i shown in Figure 2(a). Such expressions, when substituted into equation (5), yield the complete discretization equation for node i. A general representation of this equation can be cast in the following form:

$$ac_i^\phi \phi_i = \sum_{nb} ac_{nb}^\phi \phi_{nb} + b^\phi. \tag{38}$$

Discretization equations for u and v.

Except for the presence of the integrals of the pressure gradient, the integral momentum conservation equations are identical in form to the integral conservation equation for ϕ. Therefore, only the treatment of the pressure gradient term is discussed explicitly in this section. Using the specializations given in Table I, the volume integral of the source and pressure gradient terms in the z-momentum equation are approximated as

$$\int_{1aoc} S_\phi \, d\mathscr{V} = (S_{Cz})_1 \mathscr{V}_{1aoc} + (S_{Pz})_1 u_1 \mathscr{V}_{1aoc} - \left(\frac{\partial p}{\partial z}\right)_{\text{element}} \mathscr{V}_{1aoc}. \tag{39}$$

The volume integral of the source and pressure gradient terms in the r-momentum equation are approximated as

$$\int_{1aoc} S_\phi \, d\mathscr{V} = (S_{Cr})_1 \mathscr{V}_{1aoc} + (S_{Pr})_1 v_1 \mathscr{V}_{1aoc} - \left(\frac{\partial p}{\partial r}\right)_{\text{element}} \mathscr{V}_{1aoc}. \tag{40}$$

The pressure gradients in these expressions are computed using equation (27):

$$\left(\frac{\partial p}{\partial z}\right)_{\text{element}} = d, \qquad \left(\frac{\partial p}{\partial r}\right)_{\text{element}} = e. \tag{41}$$

Discretizations of the momentum equations are derived and assembled using element-by-element procedures akin to those used to obtain the discretization equation for ϕ. The resulting

u and v discretization equations for a node i can be cast in the following general forms:

$$a_i^u u_i = \sum_{nb} a_{nb}^u u_{nb} + b^u + \mathscr{V}_{CV}\left(-\overline{\frac{\partial p}{\partial z}}\right)_{CV} \tag{42}$$

$$a_i^v v_i = \sum_{nb} a_{nb}^v v_{nb} + b^v + \mathscr{V}_{CV}\left(-\overline{\frac{\partial p}{\partial r}}\right)_{CV}. \tag{43}$$

The terms $(-\overline{\partial p/\partial z})_{CV}$ and $(-\overline{\partial p/\partial r})_{CV}$ are volume-averaged pressure gradients associated with the control volume, $\mathscr{V}_{CV}$.

Interpolation of mass fluxes and discretization equation for p.

Denoting the velocity in the mass-flux terms by $\mathbf{V}^m$, the integral mass conservation equation, when applied to the control volume surrounding node i in Figure 2, can be written as follows:

$$\left[\int_a^o \rho \mathbf{V}^m \cdot \mathbf{n} 2\pi r \, ds + \int_o^c \rho \mathbf{V}^m \cdot \mathbf{n} 2\pi r \, ds\right]$$
$$+ [\text{similar contributions from other elements associated with node } i]$$
$$+ [\text{boundary contributions, if applicable}] = 0. \tag{44}$$

In each element, the velocity $\mathbf{V}^m$ can be expressed in terms of its components in the z- and r-directions, u^m and v^m, respectively, as shown in equation (10). Interpolation functions for u^m and v^m have to be prescribed in order to approximate the mass-flux integrals in equation (44). First, the discretized momentum equations, equations (42) and (43), are written in the following way:

$$u_i = \hat{u}_i + d_i^u\left(-\overline{\frac{\partial p}{\partial z}}\right)_{CV}, \qquad v_i = \hat{v}_i + d_i^v\left(-\overline{\frac{\partial p}{\partial r}}\right)_{CV}, \tag{45}$$

where

$$\hat{u}_i = \frac{\sum_{nb} a_{nb}^u u_{nb} + b^u}{a_i^u}, \qquad \hat{v}_i = \frac{\sum_{nb} a_{nb}^v v_{nb} + b^v}{a_i^v}, \tag{46}$$

$$d_i^u = \frac{\mathscr{V}_{cv}}{a_i^u}, \qquad d_i^v = \frac{\mathscr{V}_{cv}}{a_i^v}. \tag{47}$$

For the evaluation of the mass fluxes on the faces a–o and o–c in element 123 (Figure 3), the velocity components are written as

$$u^m = \hat{u} + d^u\left(-\frac{\partial p}{\partial z}\right)_{element}, \qquad v^m = \hat{v} + d^v\left(-\frac{\partial p}{\partial r}\right)_{element}, \tag{48}$$

where $\hat{u}, \hat{v}, d^u$ and d^v are interpolated linearly from the corresponding values at the vertices of the element. This interpolation for u^m and v^m is borrowed from the work of Prakash and Patankar.[15] It prevents the occurrence of spurious pressure oscillations in the proposed CVFEM. Similar interpolation of the velocity components in the mass-flux terms have been successfully used by Rice and Schnipke,[35] Peric *et al.*[36] and Rhie and Chow.[37] It should be noted, however, that this interpolation procedure may not be well suited for Newton-type linearizations of the convective terms in the momentum equations.

In the derivation of algebraic approximations to integrals of mass fluxes in equation (44), u^m and v^m are interpolated in each element by the functions given in equations (48). The same functions are also used to approximate integrals that represent the mass flow rates in the

momentum equations. They are also used to compute u_{av}^m and v_{av}^m in equation (22). Using these interpolation functions to approximate the integrals in equation (44), the contributions of element 123 (Figure 3) to the mass conservation equation for the node 1 can be expressed as

$$\int_a^o \rho \mathbf{V}^m \cdot \mathbf{n} 2\pi r \, ds = \frac{2\pi}{6}\{-y_a[\rho u_o^m(2r_o+r_a)+\rho u_a^m(2r_a+r_o)]+x_a[\rho v_o^m(2r_o+r_a)+\rho u_a^m(2r_a+r_o)]\}, \tag{49}$$

$$\int_o^c \rho \mathbf{V}^m \cdot \mathbf{n} 2\pi r \, ds = \frac{2\pi}{6}\{+y_c[\rho u_o^m(2r_o+r_c)+\rho u_c^m(2r_c+r_o)]-x_c[\rho v_o^m(2r_o+r_c)+\rho u_c^m(2r_c+r_o)]\}, \tag{50}$$

where $u_o^m, v_o^m, u_a^m, v_a^m, u_c^m$ and v_c^m are obtained using equation (48). Algebraic approximations to the mass flow rates in equation (23) are obtained analogously.

Using expressions similar to equations (12) and (13) to evaluate the pressure gradients in equation (48), and adding similar contributions of the other elements surrounding the node i, the complete discretization equation for the pressure, p, is obtained. A compact representation of the discretized pressure equation for a typical node i is the following:

$$\mathrm{ac}_i^p p_i = \sum_{\mathrm{nb}} \mathrm{ac}_{\mathrm{nb}}^p p_{\mathrm{nb}} + b^p. \tag{51}$$

3.5. *Boundary conditions*

Domain boundaries that coincide with solid walls, symmetry surfaces, inlet regions and outlet regions are considered here. All these boundaries can be accounted for in a general formulation by noting that only two types of boundary conditions are encountered: specified value or given gradient. Free-surface problems are not within the scope of this paper.

The following derivation pertains to the discretization equation for node 1 shown in Figure 3(c). The area between the points 1 and 2 is assumed to coincide with the boundary of the domain of interest.

Specified value. When the dependent variable ϕ is specified at the boundary node, and denoted as ϕ_{SP}, the discretization equation is written as follows:

$$\mathrm{ac}_i^\phi = 1, \qquad \mathrm{ac}_{\mathrm{nb}}^\phi = 0, \qquad b_i^\phi = \phi_{\mathrm{SP}}. \tag{52}$$

Specified gradient. When the gradient of the dependent variable normal to the boundary is given, say $(\partial\phi/\partial n)_{\mathrm{SP}}$, the combined convection–diffusion flux of ϕ normal to the boundary is given by

$$\mathbf{J} \cdot \mathbf{n} = \rho V_n \phi - \Gamma_\phi \left(\frac{\partial \phi}{\partial n}\right)_{\mathrm{SP}}, \tag{53}$$

where V_n is the velocity component normal to the boundary. It is assumed that the elemental values of ρ and Γ_ϕ, and the nodal value of $(\partial\phi/\partial n)_{\mathrm{SP}}$, are constant on surface 1–a. Thus, the boundary contribution to the conservation equation is given by

$$\int_1^a \mathbf{J} \cdot \mathbf{n} 2\pi r \, ds = \rho \int_1^a V_n \phi 2\pi r \, ds - \Gamma_\phi \left(\frac{\partial \phi}{\partial n}\right)_{\mathrm{SP}} \mathscr{A}_{1-a}, \tag{54}$$

where

$$\mathscr{A}_{1-a} = 2\pi l_{1-a} r_{\mathrm{m}}, \qquad l_{1-a}^2 = (r_a - r_1)^2 + (z_a - z_1)^2. \tag{55}$$

The convection contribution is evaluated using Simpson's rule, with the individual variations of V_n and ϕ approximated with linear interpolations along the element edge 1–2. The boundary contribution can finally be written as

$$\int_1^a \mathbf{J}\cdot\mathbf{n}2\pi r\,\mathrm{d}s = 2\pi l_{1-a}\left\{\frac{1}{24}[\phi_1(4\rho(V_n)_1 r_1 + 3\rho(V_n)_m r_m + 2\rho(V_n)_a r_a) + \phi_2(2\rho(V_n)_a r_a + \rho(V_n)_m r_m)] - \Gamma_\phi\left(\frac{\partial\phi}{\partial n}\right)_{SP} r_m\right\}. \tag{56}$$

This derivation has been done for the general ϕ-equation. The same treatment is also applicable to the momentum equations.

For the continuity or integral mass conservation equation, only boundaries having mass flow crossing them have non-zero contributions. With respect to link 1–a in Figure 3(c), this mass flow can be expressed as

$$\int_1^a \rho V_n 2\pi r\,\mathrm{d}s = 2\pi\frac{l_{1-a}}{6}[\rho(V_n)_1 r_1 + 4\rho(V_n)_m r_m + \rho(V_n)_a r_a]. \tag{57}$$

It should be noted here that the mass flow rates across the *boundary edges* such as 1–a in Figure 3(c), are calculated using the latest available values of the nodal velocity **V**, not $\mathbf{V}^m$. Only the mass flow rates across control-volume faces in the interior of the domain are calculated using $\mathbf{V}^m$.

Special treatments. Some special treatments are needed on *boundaries with prescribed velocities*, such as walls and inflow boundaries. At nodes which lie on such boundaries, d^u and d^v are set to zero, and, therefore

$$\hat{u} = u, \qquad \hat{v} = v. \tag{58}$$

At the *outflow boundaries*, it is assumed that diffusion is negligible. This is handled by dropping the $-\Gamma_\phi\,(\partial\phi/\partial n)$ term in equation (53).

As is well known,[31] in incompressible flow problems, the level of the pressure inside the calculation domain is unimportant. Only differences in pressure at distinct points in the domain influence the fluid flow. In the proposed CVFEM, however, it is recommended that *the value of pressure at one node be fixed to any convenient value*, for example, zero; this promotes the rate of convergence of the iterative solution algorithm, and it prevents the occurrence of excessively large levels of pressure during the solution process. In problems with inflow and outflow, the pressure should be fixed at a node located on an outflow boundary.

3.6. Solution of the discretization equations

An iterative sequential variable adjustment scheme proposed by Saabas[29] is used to solve the non-linear, coupled sets of discretization equations for u, v and p, and other dependent variables of interest.

1. Start with a guessed velocity field. Also guess values of ϕ that influence the flow field.
2. Calculate the coefficients in the momentum equations (42) and (43), without the contributions of the pressure gradient terms.
3. Calculate $\hat{u}, \hat{v}, d^u$ and d^v using equations (46) and (47).
4. Calculate the coefficients of the pressure equation (51).
5. Solve the pressure equation.
6. Complete the momentum equations by adding the pressure gradient terms, under-relax these equations, and solve for u and v.

7. For dependent variables, ϕ, that influence the flow field, calculate coefficients in the discretization equations, under-relax if required, and solve sequentially.
8. Return to Step 2 and repeat until convergence.
9. Calculate and solve discretization equations for other ϕ variables, if required.

In this work, Steps 2–8 of this procedure were repeated until the non-dimensional average residue (absolute value) for each set of discretization equations was less than 10^{-10}. Depending on the problem, global values, such as the average Nusselt number, were also monitored, and it was stipulated that the absolute value of the relative change from one iteration to the next should be less than 10^{-6}: in most of the calculations, however, it was found that the convergence criterion based on the non-dimensional average residue is more demanding.

In each cycle of this algorithm, the linearized sets of discretized equations for p, u, v and ϕ are solved sequentially. In this work, the discretized equations for u and v were under-relaxed, using the implicit under-relaxation procedure of Patankar,[31] just before they were solved. The following under-relaxation parameters were used: $\alpha_u = \alpha_v = 0{\cdot}5$. The discretized equations for p should *not be* under-relaxed. If the nodes lie along line patterns, then each of these linearized sets of equations can be solved using an iterative line-by-line tridiagonal matrix algorithm:[31] 3 repetitions of 4 alternating direction line-by-line sweeps of the calculation domain were used with each set of linearized, decoupled equations for u, v and ϕ; 10 repetitions of such sweeps were used to solve the p-equations. No special efforts were made in this work to optimize these aspects of the overall solution procedure. For unstructured grids, block-by-block or point-by-point Gauss–Seidel methods may be used to solve each of these sets of discretized equations.

To improve the rate of convergence of the aforementioned iterative solvers for the linearized discretization equations, block-correction and multigrid techniques, for example, can be included. In this work, however, these options were not considered.

4. APPLICATIONS

The validity of the proposed axisymmetric CVFEM is demonstrated in this section by its application to four different test problems, and comparisons of the solutions with available numerical and experimental results. In general, the MAW scheme produces discretized equations that are more robust than those obtained with the FLO scheme, with respect to solution with the iterative sequential algorithm discussed in the previous section. However, the results obtained with FLO, when it converges, are more accurate than those obtained with MAW, for the same grid. Therefore, most of the results presented here were obtained using the FLO scheme. However, for one of the test problems, involving laminar natural convection in a cylindrical enclosure, results obtained with both FLO and MAW are presented in order to enable a comparative evaluation of these schemes: detailed grid independence checks and CPU times are also presented for this test problem. It should also be noted that at high Reynolds numbers, good initial guess values of the u, v and p fields were essential for convergence: in such cases, a solution obtained with the MAW scheme, which is more robust but not as accurate as the FLO scheme, was fed as the initial guess to the FLO scheme.

4.1. Developing laminar flow in a pipe

Problem statement. Laminar flow of a constant-property Newtonian fluid in the inlet region of a circular pipe is investigated in this problem. The fluid enters the pipe of radius R with a uniform velocity profile: $u = \bar{u}$, $v = 0$. The ratio of the length to the radius of the pipe in this study was $L/R = 6$. The results obtained with the proposed CVFEM are compared to those of Friedmann *et al.*[38]

Governing equations. The governing equations are the z- and r-momentum and continuity equations. For negligible body force, or for body-force terms that can be absorbed into an effective pressure, the momentum equations can be written in the general form (equation (4)) using the following definition of the source term:

z-momentum

$$S_\phi = -\frac{\partial p}{\partial z}, \tag{59}$$

r-momentum

$$S_\phi = -\frac{\partial p}{\partial r} - \mu \frac{v}{r^2}. \tag{60}$$

The boundary conditions are the prescribed uniform velocity profile at the inlet, the fully developed conditions at the outlet, and the no-slip condition on the wall.

Results. The Reynolds number, $Re = \rho \bar{u} 2R/\mu$, considered in this problem is 40. A non-uniform grid, with 111 nodes in the z-direction and 61 nodes in the r-direction, was used in this test. Preliminary test with 40×15 and 56×31 grids had established that the 111×61 grid produces essentially grid-independent results: the change in $u_{min}/\bar{u}$ values produced by 56×31 and 111×61 grids is less than 0·23%. In the region $0 \leq z/R \leq 1{\cdot}25$, the u velocity profile has a local minimum on the axis of the pipe and a maximum at a value of $r > 0$. This behaviour has been observed experimentally.[39] Table II presents the local minimum and maximum u velocities at several axial locations downstream of the entrance. Table III presents a comparison of the non-dimensional hydrodynamic entrance length, defined as the distance along the axis where the centreline velocity reaches 99% of its fully developed value. The results obtained with the proposed CVFEM are compared with the finite difference solution of Friedmann *et al.*[38] The CVFEM results match the solution of Friedmann *et al.*[38] very well: the maximum percentage difference in the results presented in Table II is 0·09%; the non-dimensional hydrodynamic entrance lengths presented differ by 0·80%. This simulation illustrates the capabilities of the proposed formulation to capture accurately the fluid flow phenomena encountered in the entrance regions of pipes.

4.2. Laminar flow in a pipe with a sudden contraction

Problem statement. The behaviour of laminar flow in a straight pipe with a sudden contraction in its diameter is investigated in this problem. This simulation was conducted with the geometry proposed by Durst and Loy.[40] The inlet pipe has a diameter D of 19·1 mm, while the diameter d of the pipe after the contraction is 10·2 mm. The computational domain extends 25 mm upstream of the contraction and 20 mm downstream. At the inlet of the pipe, the flow is considered as fully developed. The length of the pipe downstream of the contraction is long enough to ensure that the following outflow treatment is satisfactory: $\partial u/\partial z = 0$ and $v = 0$.

Governing equations. The governing equations are the same as the ones presented for the developing laminar pipe flow section.

The boundary conditions are the prescribed fully developed velocity profile at the inlet, outflow treatment at the outlet, and no-slip conditions on the pipe wall.

Results. Simulations were conducted for two values of Reynolds number, Re_D, based on the inlet diameter D, namely, 196 and 968. All simulations were done with a 72×97 non-uniform grid with a concentration of nodes in the recirculating zones, one upstream and one downstream of the contraction. The presented results consist of streamlines computed using the proposed

Table II. Developing laminar flow in a pipe: u_{min} and u_{max} values

		Proposed CVFEM		Friedmann *et al.*[38]	
Re	*z/R*	$u_{min}/\bar{u}$	$u_{max}/\bar{u}$	$u_{min}/\bar{u}$	$u_{max}/\bar{u}$
40	0·25	1·048	1·219	1·048	1·219
	0·50	1·173	1·313	1·174	1·314
	0·75	1·325	1·404	1·326	1·405
	1·00	1·465	1·494	1·466	1·495
	1·25	1·579	1·583	1·580	1·583

Table III. Developing laminar flow in a pipe: non-dimensional hydrodynamic entrance length

Re	Proposed CVFEM	Friedmann *et al.*[38]
40	4·92	4·88

CVFEM, and comparisons of the computed axial and radial velocity profiles at several axial positions with the experimental data obtained by Durst and Loy.[40]

Numerical simulations on 37×51, 72×97 and 143×193 grids established that the 72×97 grid produces essentially grid-independent results. The results of this grid independence study are well illustrated by the variation of the radial velocity profile at station $z/D = -0{\cdot}052$ for the three different grids (see Figure 5(b)): one can see that the radial velocity profile predicted by the 72×97 and 143×193 grids are so close to each other that it is impossible to distinguish one from the other. All other results showed similar or better grid independence. Therefore, all other results presented in this section correspond to simulations done on the 72×97 grid.

For $Re_D = 196$, there is only one recirculating zone situated upstream of the contraction, as can be seen from the streamlines plotted in Figure 4(a). However, at $Re_D = 968$, an additional recirculating zone appears just downstream of the contraction (see Figure 4(b)). For $Re_D = 196$, Figure 5(a) presents the evolution of the axial velocity profile along the pipe: $z/D = 0$ at the location of the contraction. The agreement with the experimental data of Durst and Loy is very good: both the shape of the profiles and the magnitude of the velocity are well predicted. It is interesting to note the velocity over-shooting phenomena, exhibited by both the numerical and experimental results, just downstream of the contraction. The computed radial velocity profiles, for $Re_D = 196$, presented in Figure 5(b) do not agree as well with the experimental data: the difference in the magnitude is up to 50% at the station $z/D = -0{\cdot}052$.

The axial velocity profiles for $Re_D = 968$ are shown in Figure 6(a). The proposed CVFEM predicts a recirculating zone downstream of the contraction. This is clearly confirmed by the shape of the axial velocity profiles downstream of the contraction: a zone of negative axial velocity exists near the wall. The computations done by Durst and Loy[40] also indicate the presence of a recirculating zone downstream of the contraction. No such affirmation can be drawn from their experimental velocity profiles, however, since there are no experimental data close enough to the wall. The agreement between the CVFEM and the experimental results is again good, but not as good as in the case of $Re_D = 196$. The magnitude of the radial velocity

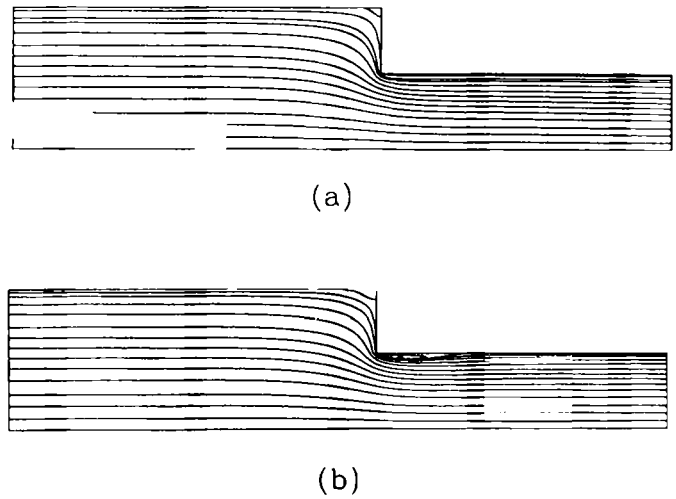

Figure 4. Streamline patterns for laminar flow in a pipe with a sudden contraction: (a) $Re_D = 196$; (b) $Re_D = 968$

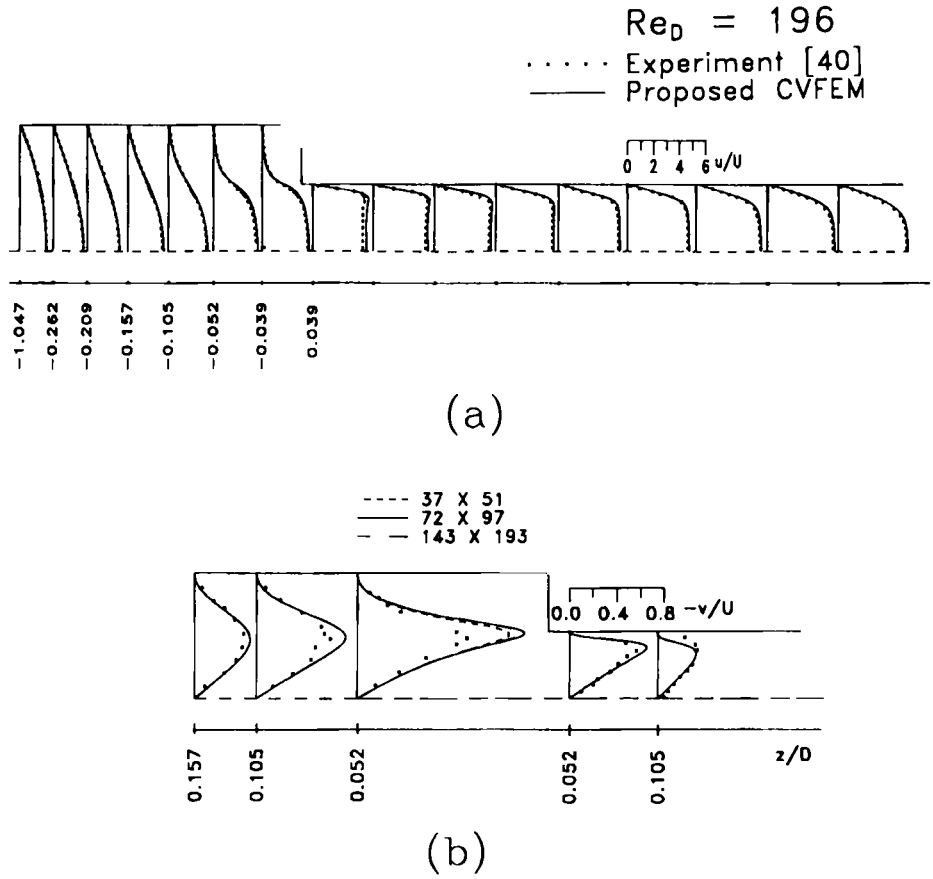

Figure 5. Laminar flow in a pipe with a sudden contraction for $Re_D = 196$: (a) axial velocity; (b) radial velocity

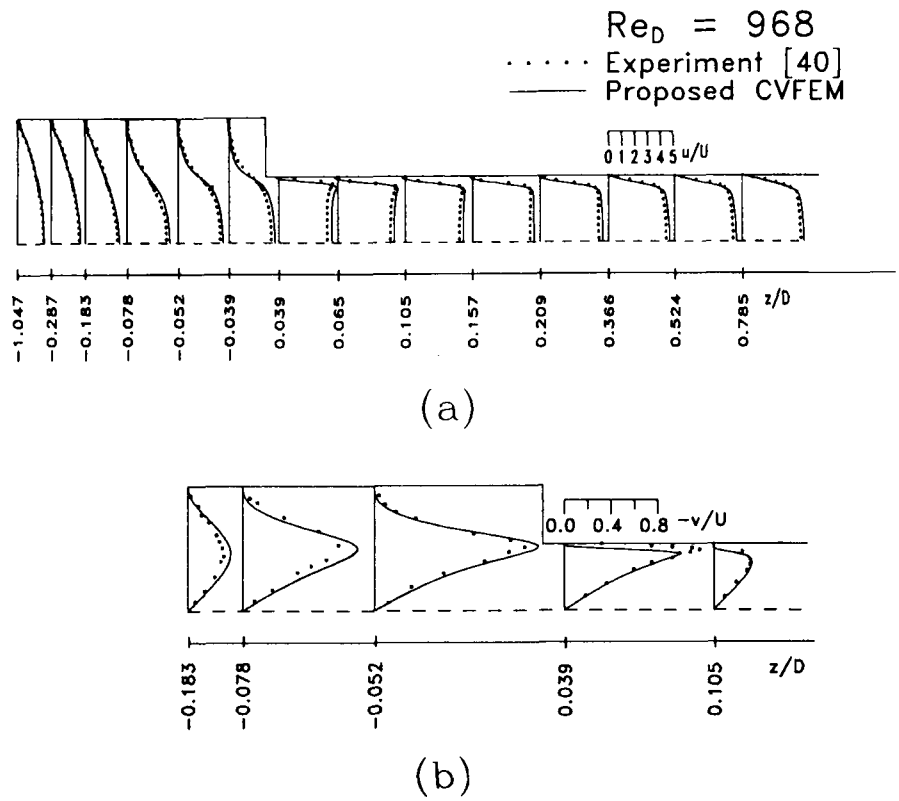

Figure 6. Laminar flow in a pipe with a sudden contraction for $Re_D = 968$: (a) axial velocity; (b) radial velocity

profiles, presented in Figure 6(b), do not agree very well with the experimental data, but the shapes of these profiles are close to the experimental ones.

4.3. *Laminar natural convection in a cylindrical enclosure*

Problem statement. Axisymmetric buoyancy-driven laminar flow in a cylindrical cavity is presented in this section. This problem is schematically illustrated in Figure 7. A Newtonian fluid, with a temperature-dependent viscosity, is confined within the cylindrical region $0 \leq r \leq R$, $0 \leq z \leq L$. The lateral boundary, $r = R$, is insulated, and the horizontal surfaces $z = 0$ and $z = L$ are maintained, respectively, at constant temperatures T_H and T_C, where $T_H > T_C$. The acceleration due to gravity, **g**, is directed in the negative z-direction. The results obtained with the proposed CVFEM are compared with those obtained by Liang *et al.*[41] using a Finite Difference Method (FDM).

Governing equations. In this problem, the governing equations are the z- and r-momentum, continuity and energy equations. The Boussinesq approximation is used: thus, density is assumed to be a constant, $\rho = \rho_0$, in all terms, except the buoyancy term in the z-momentum equation, in which $\rho = \rho_0(1 - \beta(T - T_H))$. Here, β is the thermal volumetric expansion coefficient of the fluid. The specific heat, C_P, and the thermal conductivity, k, of the fluid are assumed to remain constant.

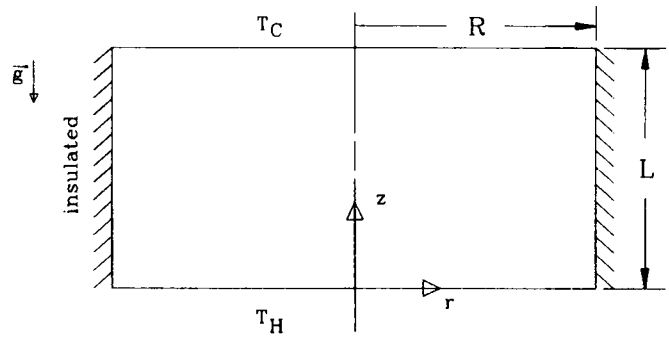

Figure 7. Schematic representation of laminar natural convection in a cylindrical enclosure

The source terms in the momentum equations can be written as follows:

z-momentum

$$S_\phi = -\frac{\partial p}{\partial z} - \rho_0 g + \beta g \rho_0 (T - T_H) + \frac{\partial \mu}{\partial z}\frac{\partial u}{\partial z} + \frac{\partial \mu}{\partial r}\frac{\partial v}{\partial z}, \tag{61}$$

r-momentum

$$S_\phi = -\frac{\partial p}{\partial r} - \mu\frac{v}{r^2} + \frac{\partial \mu}{\partial z}\frac{\partial u}{\partial r} + \frac{\partial \mu}{\partial r}\frac{\partial v}{\partial r}. \tag{62}$$

The temperature distribution is governed by the *energy equation*

$$\frac{\partial}{\partial z}(\rho_0 u T) + \frac{1}{r}\frac{\partial}{\partial r}(r\rho_0 v T) = \frac{\partial}{\partial z}\left(\rho_0 \alpha \frac{\partial T}{\partial z}\right) + \frac{1}{r}\frac{\partial}{\partial r}\left(r\rho_0 \alpha \frac{\partial T}{\partial r}\right), \tag{63}$$

where α is the thermal diffusivity of the fluid ($\alpha = k/\rho_0 C_P$).

In accordance with the assumptions of Liang *et al.*,[41] viscosity is a function of temperature, according to the following expression:

$$\mu = \mu_C\left(1 + \eta\frac{T - T_C}{T_H - T_C}\right), \tag{64}$$

where η is a parameter for this problem. The other non-dimensional parameters are R/L, the Prandtl number, Pr, and the Grashof number, Gr:

$$Pr = \frac{\mu_C}{\rho_0 \alpha}, \qquad Gr = \frac{g\beta(T_H - T_C)L^3\rho_0^2}{\mu_C^2}. \tag{65}$$

Results. Two steady-state regimes, one with upflow and the other with downflow at the axis, were found experimentally and numerically.[41] Numerically, a specific steady-state regime is simulated by using the proper initial temperature distribution. To get upflow at the axis, the lighter fluid (hot fluid) has to be near the axis initially. For the downflow solution, the heavier fluid (cold fluid) has to be near the axis. The numerical results presented in this section were computed for $R/L = 1$, $Pr = 2500$, $Gr = 2$ and $\eta = -0{\cdot}2$. Preliminary computations on uniform 11×11, 31×31 and 51×51 grid (see Figure 8) demonstrate that the 51×51 grid is fine enough to get grid-independent results when the FLO scheme is used. Figure 8 also presents the numerical

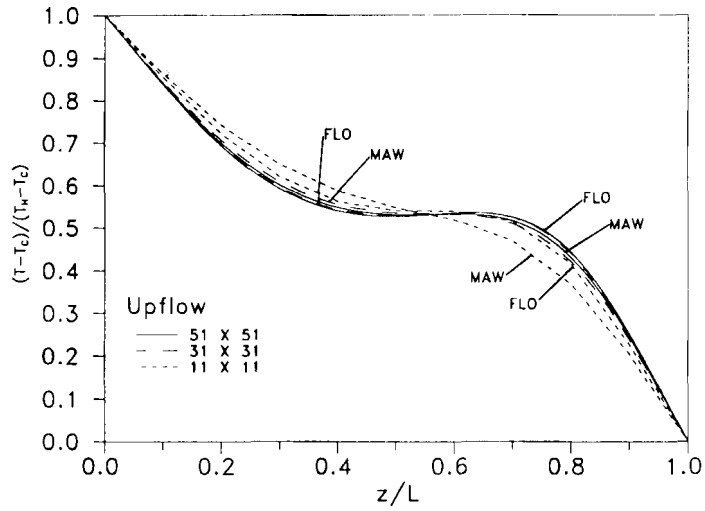

Figure 8. Temperature distribution along $r/R=0{\cdot}5$ in laminar natural convection in a cylindrical enclosure: grid-independence study for the case of upflow using FLO and MAW

results obtained with the MAW scheme. As was expected, with the coarse grid (11×11), the MAW-scheme solution is not as accurate as that of the FLO scheme. For the grid which is considered to produce grid-independent results with the FLO scheme (51×51), the solution obtained with the MAW scheme is in pretty good agreement with the FLO-scheme solution. However, the solution of the MAW scheme on the 51×51 grid is not as grid-independent as that of the FLO scheme. In terms of convergence, this test problem is more challenging than the other three test problems presented in this paper. Accordingly, the number of iterations and the CPU times needed to achieve convergence are presented only for this test problem, both for the FLO and the MAW schemes (see Table IV). A Hewlett-Packard HP-720 Unix-based workstation was used to solve this problem, with a HP FORTRAN 77 compiler running at optimization level 3. Convergence was considered to be achieved when both the absolute value of the relative change in the average Nusselt number and the non-dimensional average residue of all the equations were less than 10^{-6} and 10^{-10}, respectively. The temperature distributions for the upflow and downflow regimes are presented in Figure 9(a) and 9(b). The solutions given by the proposed CVFEM are in good agreement with the numerical results obtained by Liang *et al.*[41]

Table V gives a comparison of the average Nusselt numbers, Nu, computed by the proposed CVFEM and the FDM of Liang *et al.*[41] The average Nusselt number is given by

$$Nu=\frac{QL}{\pi R^2 k(T_H-T_C)}, \tag{66}$$

where Q is the overall rate of heat transfer through the top or bottom surface. The CVFEM Nusselt numbers are grid-independent extrapolated values obtained as follows:

$$Nu_{gi}=Nu_c+K\delta^n \tag{67}$$

where Nu_{gi} is the grid-independent Nusselt number, Nu_c is the computed Nusselt number, and δ is the grid size ($\Delta r=\Delta z=$ const.). For a given set of parameters, the unknowns in this equation are Nu_{gi}, K and n. Therefore, three calculations, on three different grids, provide enough

Table IV. Laminar natural convection in a cylindrical enclosure: number of iterations and CPU times

Scheme	Grid	Iterations	CPU time (s)
FLO	11 × 11	139	7·7
FLO	31 × 31	972	534·3
FLO	51 × 51	2510	3960·2
MAW	11 × 11	158	5·7
MAW	31 × 31	1017	438·0
MAW	51 × 51	2577	3195·1

extrapolation equations to find the unknowns. In equation (67), it is assumed that terms of order δ^{n+1} are negligible. To confirm that this indeed was the case, a fourth calculation, with a 61×61 grid, was done. Two extrapolated values, computed using the first three and the last three computations, were obtained; they were invariant to four significant figures.

The slight discrepancy between the Nusselt number predicted by the proposed CVFEM and FDM of Liang *et al.*[41] can be partly explained by noting the use of a non-conservative formulation in the FDM.[41] This non-conservative FDM yields different Nusselt numbers at the top and bottom surfaces, while the proposed conservative CVFEM gives the same Nusselt number. Since the lateral wall of the container is insulated, the top and bottom Nusselt numbers should be equal. A difference between the top and bottom Nusselt numbers implies a heat flux through the lateral wall, which is in contradiction with the prescription of the problem.

4.4. Laminar flow in a replica segment of a coronary artery

Problem statement. In this problem, laminar flow in a replica segment of a mildly atherosclerotic human coronary artery is simulated. Mild atherosclerosis corresponds to a maximum obstruction in the artery of about 50% by cross-sectional area. In the investigation of Back *et al.*,[42] two replicas of a coronary artery were used. The first one was a hollow cast of a segment of the left circumflex coronary artery of a man with mild atherosclerosis. The second was an axisymmetric analogue of the original casting: the analogue casting had a straight axis, and the same cross-sectional area as the original casting at corresponding axial locations. A schematic representation of the analogue casting is presented in Figure 10. More recently, Back *et al.*[43] did a steady-state flow test in the analogue replica. In this section, a numerical simulation, using the proposed CVFEM, of fluid flow in the analogue replica will be presented, along with a comparison with the experimental results of Back *et al.*[43]

Governing equations. The experiments of Back *et al.*[43] were done with a 33% sugar–water solution. The resulting fluid can be considered as Newtonian and, therefore, the governing equations are the same as the Navier–Stokes equations enumerated earlier in the context of developing laminar pipe flow.

The boundary conditions are the prescribed Poiseuille velocity profile at the inlet, the outflow treatment at the outlet, and the no-slip condition on the wall.

Results. Figure 10 illustrates the analogue geometry: It is important to note that the scale in the radial direction is ten times bigger than the axial scale. This geometry is clearly irregular, and it has been chosen to illustrate the capability of the proposed CVFEM to simulate flow in a complex geometry. A grid independence analysis was done for a Reynolds number, based on average velocity and diameter at the inlet, of 353. Pressure coefficients ($=[p-p_{z=0}]/[0{\cdot}5\rho u_{\mathrm{av}}^2]$)

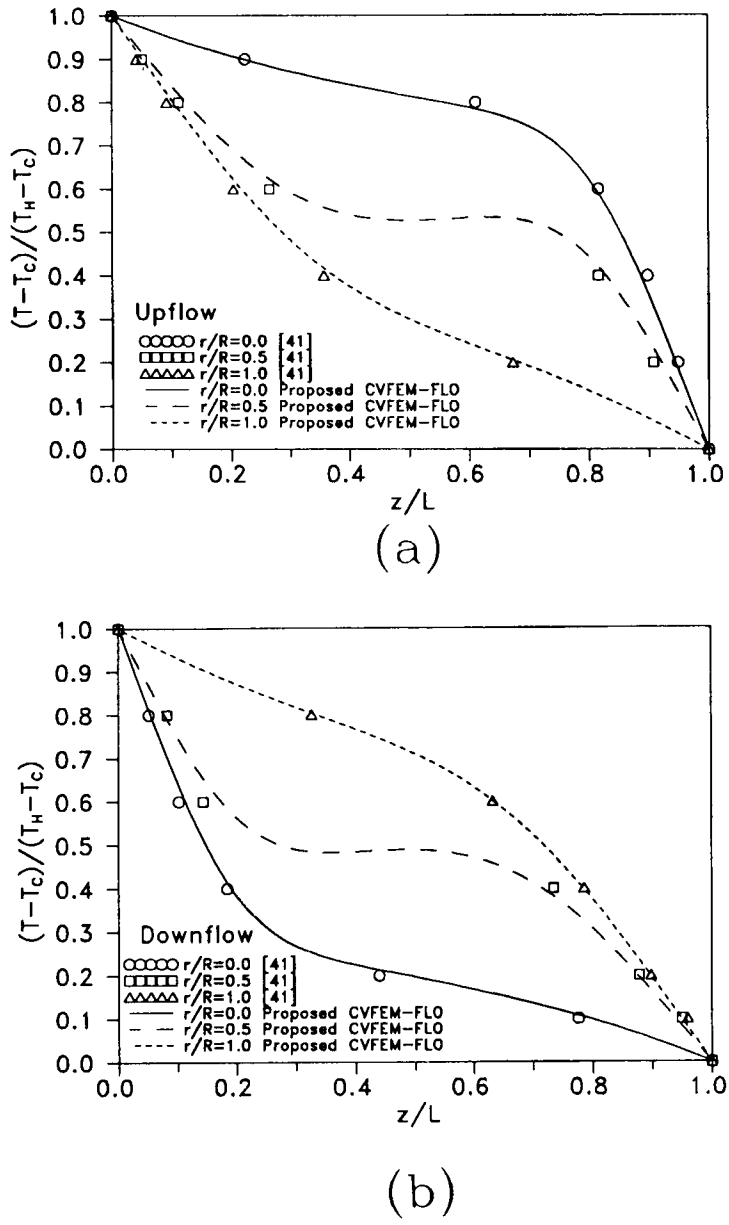

Figure 9. Temperature distribution in laminar natural convection in a cylindrical enclosure: (a) upflow; (b) downflow

Table V. Laminar natural convection in a cylindrical enclosure: average Nusselt number results

Case	Proposed CVFEM	Liang *et al.*[41]
Upflow	1·768	1·767
Downflow	1·765	1·761

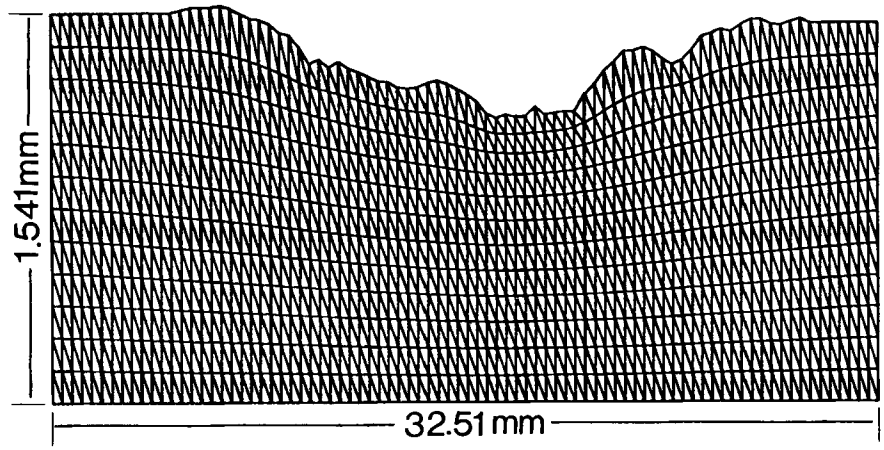

Figure 10. Straight axisymmetric analogue casting of a coronary artery and the grid: scale in radial direction is ten times than that in the axial direction

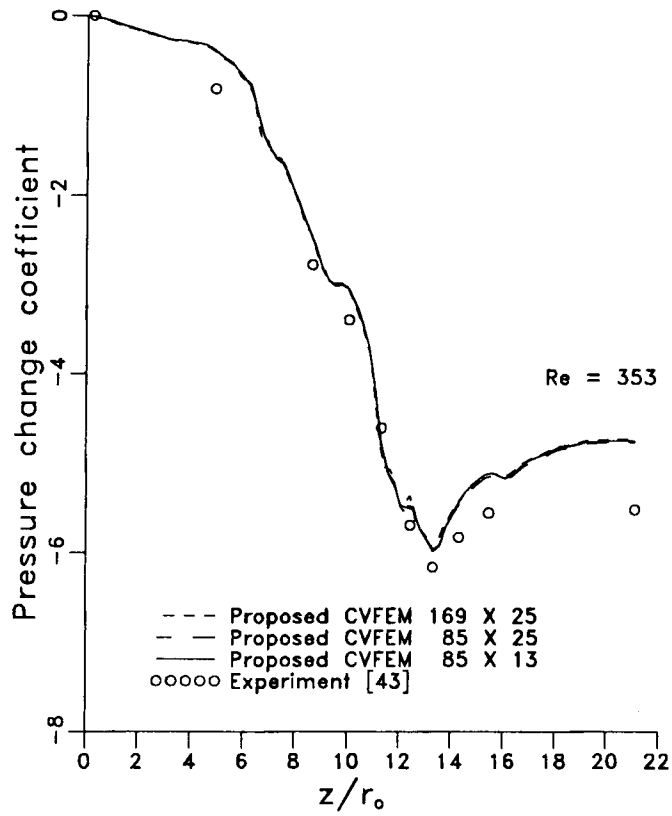

Figure 11. Laminar flow in a replica segment of a coronary artery: pressure-change coefficient for different grids

obtained in this analysis are presented in Figures 11 and 12. In Figure 11, it is seen that the results obtained using a 85×13 grid is close to that obtained on a 169×25 grid. Based on this comparison, the 85×13 grid, presented in Figure 10, was used for all the other calculations. Figure 12 presents a comparison between the numerical results obtained using the proposed

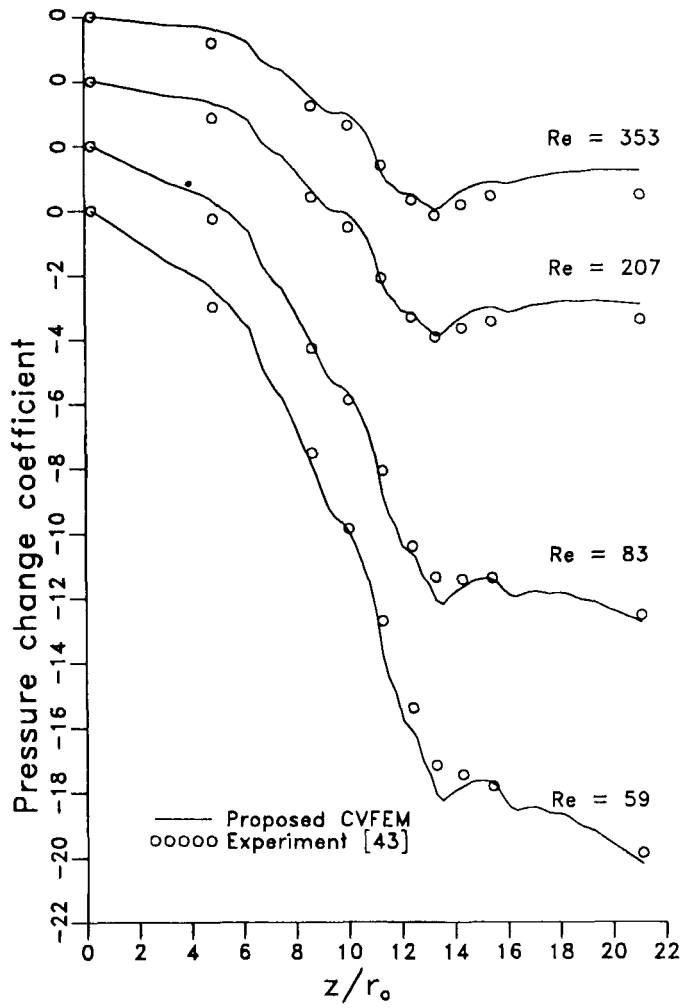

Figure 12. Laminar flow in a replica segment of a coronary artery: pressure-change coefficient for different Reynolds numbers

CVFEM and the experimental data of Back *et al.*[43] for $Re = 59, 83, 207$ and 353. The agreement of the numerical results with the experimental data is good.

5. CONCLUSION

In this paper, the formulation and the capabilities of a co-located, equal-order CVFEM for steady, axisymmetric, incompressible fluid flow and heat transfer problems have been presented. Independent numerical and experimental investigations available in the literature have been used to check the results of the proposed CVFEM. These comparisons indicate that the proposed CVFEM can successfully solve elliptic, axisymmetric, incompressible fluid flow and heat transfer problems in regular and irregular geometries. The test problems presented in this paper involved only laminar flow in singly connected domains discretized using structured grids. This is a limitation of the implementation. The proposed method has no such limitation in principle.

ACKNOWLEDGEMENTS

The support of the Natural Sciences and Engineering Research Council of Canada (NSERC), in the form of a Postgraduate Scholarship to the first author and an operating grant to Prof. Baliga, is gratefully acknowledged. The research activities of Prof. Baliga are also supported by the Centre de Recherche en Calcul Appliqué (CERCA) in Montréal, Québec.

REFERENCES

1. B. A. Finlayson and L. E. Scriven, 'The method of weighted residuals—a review', *Appl. Mech. Rev.*, **19**, 735–748 (1966).
2. O. C. Zienkiewicz, *The Finite Element Method*, McGraw-Hill, London, 1977.
3. F. H. Harlow and J. E. Welch, 'Numerical calculation of time-dependent viscous incompressible flow of a fluid with free surface', *Phys. Fluids*, **8**, 2182–2189 (1965).
4. S. V. Patankar and D. B. Spalding, 'A calculation procedure for heat, mass and momentum transfer in three-dimensional parabolic flows', *Int. J. Heat Mass Transfer*, **4**, 551–559 (1972).
5. G. D. Raithby, 'Skew upstream differencing schemes for problems involving fluid flow', *Comput. methods appl. mech. eng.*, **9**, 153–164 (1976).
6. B. R. Baliga, 'A control-volume-based finite element method for convective heat and mass transfer', *Ph.D. Thesis*, University of Minnesota, MN, 1978.
7. S. Ramadhyani, 'Solution of the equations of convective heat, mass and momentum transfer by finite element method using quadrilateral elements', *Ph.D. Thesis*, University of Minnesota, MN, 1979.
8. C. Prakash, 'A finite element method for predicting flow through ducts with arbitrary cross-sections', *Ph.D. Thesis*, University of Minnesota, MN, 1981.
9. A. M. Winslow, 'Numerical solution of the quasilinear Poisson equation in a nonuniform mesh', *J. Comput. Phys.*, **2**, 149–172 (1967).
10. J. T. Oden, 'Finite element analogue of Navier–Stokes equation', *J. eng. mech. div. ASCE*, **96** (EM4), 529–534 (1970).
11. C. Taylor and P. Hood, 'A numerical solution of the Navier–Stokes equations using the finite element technique', *Comput. Fluids*, **1**, 73–100 (1973).
12. B. R. Baliga and S. V. Patankar, 'A new finite-element formulation for convection–diffusion problems', *Numer. Heat Transfer*, **3**, 393–409 (1980).
13. B. R. Baliga and S. V. Patankar, 'A control-volume finite element method for two-dimensional fluid flow and heat transfer', *Numer. Heat Transfer*, **6**, 245–261 (1983).
14. B. R. Baliga and S. V. Patankar, 'Elliptic systems: finite element method II', in W. J. Minkowycz *et al.* (eds), *Handbook of Numerical Heat Transfer*, Chapter 11, Wiley, New York, 1988, pp. 421–461.
15. C. Prakash and S. V. Patankar, 'A control volume-based finite-element method for solving the Navier–Stokes equations using equal-order velocity–pressure interpolation', *Numer. Heat Transfer*, **8**, 259–280 (1985).
16. B. LeDain-Muir and B. R. Baliga, 'Solution of three-dimensional convection–diffusion problems using tetrahedral elements and flow-oriented upwind interpolation functions', *Numer. Heat Transfer*, **9**, 143–162 (1986).
17. C. Prakash, 'An improved control volume finite-element method for heat and mass transfer, and for fluid flow using equal-order velocity–pressure interpolation', *Numer. Heat Transfer*, **9**, 253–276 (1986).
18. N. A. Hookey and B. R. Baliga, 'Evaluation and enhancements of some control-volume finite element methods: Part II—fluid flow problems', *Numer. Heat Transfer*, **14**, 273–293 (1988).
19. G. E. Schneider and M. J. Raw, 'A skewed positive influence coefficient upwinding procedure for control volume base finite element convection diffusion computation', *Numer. Heat Transfer*, **9**, 1–26 (1986).
20. G. E. Schneider and M. J. Raw, 'Control-volume finite-element method for heat transfer and fluid flow using colocated variables –1. Computational procedure', *Numer. Heat Transfer*, **11**, 363–390 (1987).
21. V. A. F. Costa and L. A. Oliveira, 'A control volume based finite element method for two-dimensional steady fluid flow, heat transfer, and related phenomena', *Proc. III Portuguese Conference on Computation Mechanics*, Coimbra, Portugal, 1992, F10.1–F10.15.
22. D. Elkaim, M. Reggio and R. Camarero, 'Simulating two-dimensional turbulent flow by using the k–ε model and the vorticity–streamfunction formulation', *Int. j. numer. methods fluids*, **14**, 961–980 (1992).
23. S. Choudhury and R. A. Nicolaides, 'Discretization of incompressible vorticity–velocity equations on triangular meshes', *Int. j. numer. methods fluids*, **11**, 823–833 (1990).
24. B. van Leer, 'Towards the ultimate conservative difference schemes—V. A second-order sequel to Gudunov's method', *J. Comput. Phys.*, **32**, 101–136 (1979).
25. A. Jameson and D. Mavriplis, 'Finite volume solution of the two-dimensional Euler equations on a regular triangular mesh', *AIAA Paper 85-0435*, 1985.
26. A. Lahrmann, 'An element formulation for the classical finite difference and finite volume method applied to arbitrarily shaped domains', *Int. j. numer. methods eng.*, **35**, 893–913 (1992).
27. C. R. Swaminathan and V. R. Voller, 'Streamline upwind scheme for control-volume finite elements, Part I. Formulations', *Numer. Heat Transfer* (Part B) **22**, 95–107 (1992).

28. N. A. Hookey, 'A CVFEM for two-dimensional viscous compressible fluid flow', *Ph.D. Thesis*, Department of Mechanical Engineering, McGill University, Montreal, Canada, 1989.
29. H. J. Saabas, 'A control volume finite element method for three-dimensional, incompressible, viscous fluid flow', *Ph.D. Thesis*, Department of Mechanical Engineering, McGill University, Montreal, Canada, 1991.
30. B. R. Baliga and H. J. Saabas, 'Control-volume finite element methods for incompressible fluid flow', *Proc. III Portuguese Conference on Computational Mechanics*, Keynote Lecture on Fluid Dynamics, Coimbra, Portugal, 1992, C2.1–C2.20.
31. S. V. Patankar, *Numerical Heat Transfer and Fluid Flow*, McGraw-Hill, New York, 1980.
32. T. J. Barth, 'On unstructured grids and solvers', in *Computational Fluid Dynamics*, Von Karman Institute Lecture Series, 1990-03, 1990.
33. Y. A. Hassan, J. G. Rice and J. H. Kim, 'A stable mass-flow-weighted two-dimensional skew upwind scheme', *Numer. Heat Transfer*, **14,** 395–408 (1983).
34. C. Prakash, 'Examination of the upwind (donor-cell) formulation in control volume finite-element methods for fluid flow and heat transfer', *Numer. Heat Transfer*, **11,** 401–416 (1987).
35. J. G. Rice and R. J. Schnipke, 'An equal-order velocity–pressure formulation that does not exhibit spurious pressure modes', *Comput. methods appl. mech. eng.*, **58,** 135–149 (1986).
36. M. Peric, R. Kessler and G. Scheuerer, 'Comparison of finite-volume numerical methods with staggered and co-located grids', *Comput. Fluids*, **16,** 389–403 (1988).
37. C. M. Rhie and W. L. Chow, 'Numerical study of the turbulent flow past an airfoil with trailing edge separation', *AIAA J.*, **21,** 1525–1532 (1983).
38. M. Friedmann, J. Gillis and N. Liron, 'Laminar flow in a pipe at low and moderate Reynolds numbers', *Appl. Sci. Res.*, **19,** 426–438 (1968).
39. J. P. Burke and N. S. Berman, 'Entrance flow development in circular tubes at small axial distances', *ASME Paper 69-WA/FE-13*, 1969.
40. F. Durst and T. Loy, 'Investigations of laminar flow in a pipe with sudden contraction of cross sectional area', *Comput. Fluids*, **13,** 15–36 (1985).
41. S. F. Liang, A. Vidal and A. Acrivos, 'Buoyancy-driven convection in cylindrical geometries', *J. Fluid Mech.*, **36,** 239–256 (1969).
42. L. H. Back, Y. I. Cho, D. W. Crawford and R. F. Cuffel, 'Effect of mild atherosclerosis on flow resistance in a coronary artery casting of man', *J. Biomech. Eng.*, **106,** 48–53 (1984).
43. L. H. Back, J. R. Radbill, Y. I. Cho and D. W. Crawford, 'Measurement and prediction of flow through a replica segment of a mildly atherosclerotic coronary artery of man', *J. Biomech.*, **19,** 1–17 (1986).